Nondestructive Evaluation of Spot Welds Using Acoustic and Thermographic Imaging Techniques

Daniel Türler, Deborah Hopkins, Frédéric Reverdy

Lawrence Berkeley National Laboratory

1 Cyclotron Road

Berkeley, CA 94720

ABSTRACT

A series of laboratory experiments were conducted to determine the ability of acoustic and thermographic methods to evaluate the quality of individual spot welds and the structural integrity of spot-welded joints with and without adhesive. Test specimens consisted of spot-welded, adhesive-bonded, and weld-bonded lap joints in steel plates. The quality of the spot welds was altered by varying welding parameters. After nondestructive evaluation, the samples were peeled or subjected to mechanical tests to determine the strength of the welds. Results demonstrate that it is possible to detect defective spot welds in both the thermographic and acoustic images. Techniques are presented that allow identification of "stick" welds characterized by solid but weak contact. Methods to quantify the imaging results are being developed by comparing the acoustic and thermographic images to the data obtained from mechanical strength tests and modeling results.

INTRODUCTION

The work presented here is part of a larger research effort focused on development of nondestructive evaluation (NDE) and testing techniques that are sufficiently fast, robust, accurate, and cost-effective to be suitable for on-line inspection of automotive structures. Developing sensors and analysis software that are necessary for real-time diagnostic evaluation are important components of the research. Analytical and numerical models are also being developed to help guide and interpret the results of the laboratory experiments. The insight and knowledge gained from these tools is essential in moving from qualitative techniques that identify flaws to quantitative methods that assess the severity of defects.

The laboratory experiments and modeling work described herein are being performed to better understand the acoustic and thermal behavior of spot welds and spot-welded joints with the goal of improving existing inspection methods, and developing next-generation techniques that are suitable for lightweight materials and new welding and joining technologies.

This requires a better understanding of how nondestructive measurements are affected by surface coatings, inclusions and voids, deformation of the sheets that occurs during welding, and surface roughness and the weld indentation. Lightweight materials such as aluminum present additional challenges, in part because they are joined using new technologies such as laser welding and weldbonding (spot welds used in conjunction with adhesive).

One approach to on-line inspection is development of techniques that provide data for a quick go/no-go decision. Once a damaged structure has been pulled off the assembly-line, subsequent testing can employ higher resolution scanning methods that are capable of locating and imaging the defects. High-resolution acoustic and thermographic techniques are presented for the characterization of individual spot welds. Particular emphasis is placed on the identification of structurally weak welds that can be more difficult to detect than broken or undersized welds.

The thermographic and acoustic data are compared to the peak loads measured for spot welds that were subjected to mechanical testing, and to measurements of the size of weld nuggets made after peeling spot-welded joints. These results are being used to help quantify the relationships between weld characteristics, weld strength, nugget diameter, and acoustic and thermographic data. Results presented in the last section of the paper demonstrate the sensitivity of global acoustic methods to the quality of welds on spot-welded joints. While individual spot welds might be difficult to inspect online because of time and access constraints, global methods are fast, require limited access to parts, and are well suited for on-line detection of weak joints because of their sensitivity to structural stiffness.

CONVENTIONAL SPOT-WELD INSPECTION

The most common methods for monitoring spot-weld integrity in manufacturing operations are pry checks and physical teardown, during which spot welds are pried apart and visually inspected or measured with calipers [1]. Although these methods have been used

successfully for decades, destructive testing has several drawbacks including high costs associated with scrapped material, ergonomic injuries, and the time lag between the onset and identification of problems. In addition, pry tests and teardowns do not allow plant managers and engineers to easily collect inspection data that would allow them to identify trends and potential problems.

PREVIOUS WORK IN NDE OF SPOT WELDS

In previous work by LBNL and others, various NDE methods including x-ray, magnetic, laser-ultrasonic, ultrasonic guided-wave, acoustic microscopy, resonance, and thermographic techniques have been employed to inspect spot-welded joints [2,3,4,5]. Although these studies have provided valuable information about identifying and characterizing weld defects, they are not practical methods for use in manufacturing environments. For example, x-ray experiments are bulky, costly, require safety precautions, and cannot distinguish between satisfactory and cold welds. Magnetic measurements are very sensitive to surface roughness and the weld indentation. Laser-ultrasonic methods are costly, and require safety precautions and a lengthy inspection time. Guided waves cannot distinguish between satisfactory and cold welds. Thermographic techniques and acoustic microscopy, including their relative advantages and disadvantages, are discussed in the following sections.

COMMERCIALLY AVAILABLE SPOT-WELD INSPECTION SYSTEMS

The most enabling technology to date is a high-frequency ultrasonic probe working in pulse-echo mode [6]. Although commercially available systems are successfully used in European plants, they have not been widely adopted in the U.S. Most commercial ultrasonic systems characterize welds based on analysis of changes in the acoustic signal resulting from structural changes in the weld nugget that occur during the welding process. On the plus side, the systems are relatively inexpensive, and well tested. On the negative side, they require trained operators to achieve satisfactory results. Operators must manipulate the probe to obtain an acceptable signal, and program the system to set threshold values and "gates" that are the basis for characterizing welds. In positioning the sensor, both perpendicularity and lateral placement are critical to record a signal representative of the spot-weld structure. The operator must also change probes depending on the size of the weld; it is not uncommon for welds on a single part to require several probe sizes.

EVALUATION OF STICK WELDS

A well-known problem in the evaluation of spot welds is the difficulty of detecting so-called "stick welds," characterized by solid but weak contact. Although structurally weak, stick welds provide good contact between the two surfaces being joined, and thus conduct heat and acoustic energy across the joint in a manner similar to strong welds.
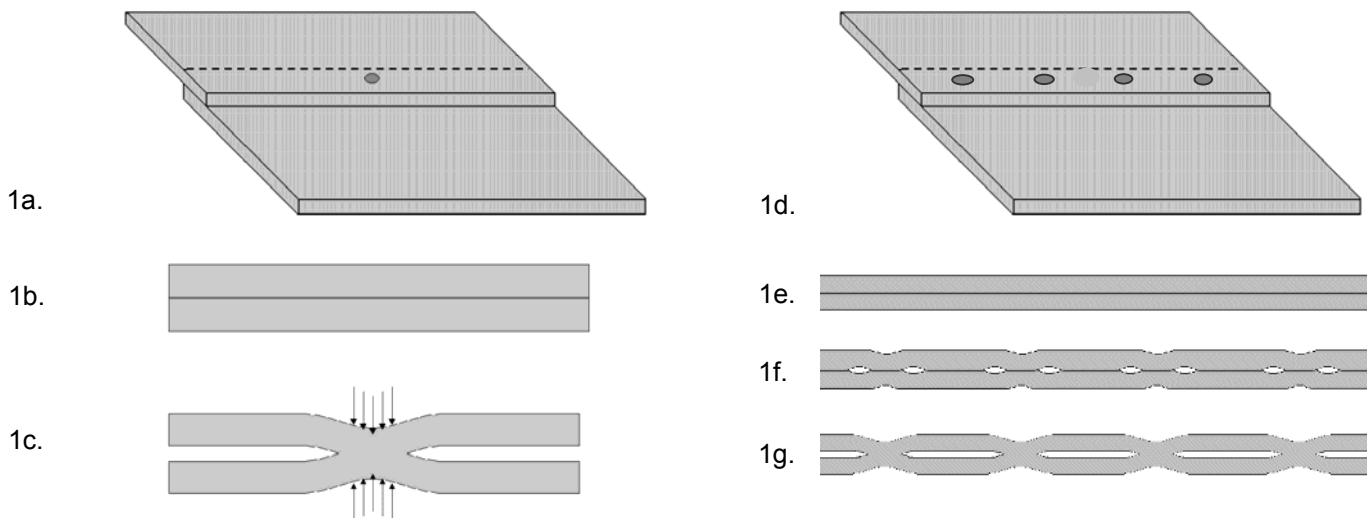

Figure 1. Schematic diagrams of two plates joined by a lap joint (1a and 1b). Before welding, the plates overlap with nominally uniform contact as illustrated for a two-dimensional slice through the center of the joint (1b and 1e). As the weld nugget forms, the joint surfaces deform (1c). Weak spot welds cause minimal deformation of the joint surfaces (1f) compared to the deformation that occurs with strong welds (1g).

As will be shown in the following sections, stick welds can be identified by both local methods in which individual welds are evaluated, and by global methods in which the entire spot-welded joint is evaluated.

JOINT DEFORMATION

The spot welding process deforms the joint surfaces creating gaps between the metal plates in the areas surrounding the spot welds. Consider a lap joint between two metal plates as illustrated in Figure 1a. Before welding, the flat metal plates overlap over the area of the joint with nominally uniform contact, as indicated in Figure 1b for a two-dimensional slice through the center of the joint. As the weld nugget forms, the joint surfaces deform as indicated in Figure 1c. Weak spot welds cause minimal deformation of the joint surfaces (Figure 1e) compared to the deformation that occurs with strong welds (Figure 1f). As a result, there tends to be greater contact area over the joint surface for plates joined with weak spot welds than with strong welds. Since the areas of contact between the welds conduct heat and acoustic energy across the joint, caution must be exercised when interpreting acoustic and thermographic data. Joints with very weak spot welds may conduct heat and acoustic energy as well or better than joints with strong spot welds.

TEST SPECIMENS

Various test specimens were used in the laboratory experiments conforming to either ASTM or industry standards. For the first series of thermography experiments and global resonance tests, the test specimens were composed of two uncoated low-carbon steel plates 0.86-mm thick, joined by a lap joint (see Figure 2a). The joints were spot welded, adhesive-bonded, or weldbonded. Welbonding consists of bonding joints with epoxy-based adhesives, then making resistance spot welds through the adhesive layer.

The spot-welded joints were prepared according to the standards specified by the American Welding Society (AWS) for tension/shear test specimens. The weld-bonded test specimens were fabricated according to standard ASTM D 1002-94 for adhesive bonding (Figure 2a) and the AWS spot-welding standards (Figure 2b). The quality of the spot welds was altered by varying the number of cycles and the current used during welding. The four combinations of settings used are shown in Table 1 and are labeled as Types I-IV for ease of reference.

For the experiments using pulsed-phased thermography, the samples were 1.4-mm-thick sheets made of galvanized steel. The acoustic microscopy measurements were made on a stainless-steel test specimen with five spot welds. The quality of the welds was varied by varying the value of the welding current. To eliminate surface effects, the outer surfaces of the sample were polished to eliminate the indentations caused by the welding electrodes.

STRENGTH TESTS

After nondestructive evaluation of the plates using thermographic techniques, the plates were cut into strips as indicated in Figure 2a to obtain the samples that were subjected to mechanical testing. This procedure is in accordance with the ASTM standard for weldbonding, which recommends that test specimens be cut from plates with not less than five specimens. Once cut, the individual samples were machined to remove burrs and smooth sharp edges. For the adhesive-bonded samples, the specimens at the edges of the plate (shaded areas in Figure 2a) were not used for mechanical testing to avoid any irregularities in the adhesive layer that sometimes occur near the edges of the plates.

The spot-welded samples were tested in shear to failure according to ASTM standards (ASTM D 1002-72), with a 1.3 mm/min pulling rate. The average maximum load achieved for each of the four combinations of welding parameters is shown in Table 1. Of the 30 spot welds tested, only two failed at the sheet. All others failed at the weld indicating that they were weak stick welds. The welds were purposely designed to be relatively weak because the experiments were focused on studying the ability of NDE methods to identify stick welds. The failure behavior of the welds tested in shear does not result in a weld nugget, so the results cannot be directly compared to the results of peel tests.

THERMOGRAPHIC TECHNIQUES

Infrared thermography is particularly well suited to inspection of structures with adhesive-bonded joints, for example, large structures such as truck beds made from adhesive-bonded composites [7]. For many potential structural automotive applications, adhesive-bonded joints would be held in place with spot welds until the adhesive is cured. In these applications, detecting damage in the adhesive layer caused by the spot-welding process is more important than assessing the structural integrity of the welds.

Infrared (IR) thermography is a fast, noncontact, full-field imaging technique. IR imaging radiometers measure thermal radiation energy and are used to detect and characterize defects in a wide range of materials. The method requires that a heat flow be established by heating one side of the test specimen and cooling the opposite side. Any change in thermal resistance in the direction of the heat flux results in a change in the temperature gradient. A suitable IR camera can detect temperature differences of less than 0.1ºC and visualize voids and defects for surface emittances greater than 0.7. Measured surface temperatures can be used to image voids and defects even at depth [8]. The resolvable flaw size depends on the thickness and thermal conductivity of the material.
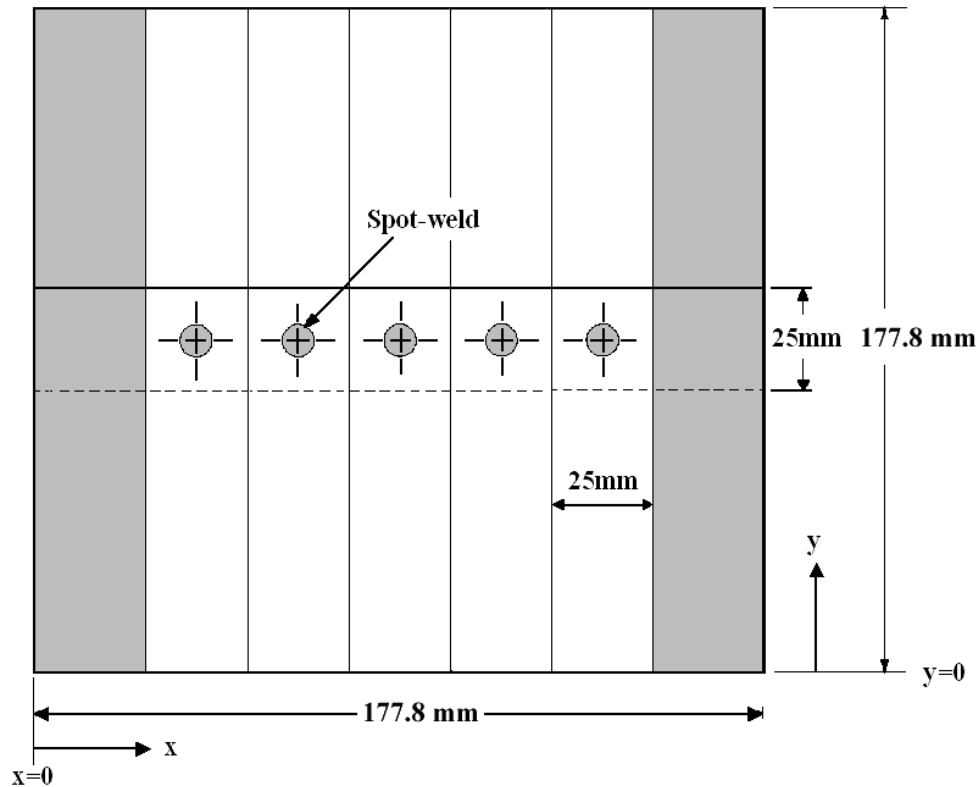
Figure 2a. Schematic diagram of the test specimens used for the thermographic and acoustic resonance measurements showing the dimensions of the lap joint and the positions of the welds on the spot-welded joints. The vertical lines indicate where the plates were cut to make the individual specimens subjected to mechanical strength testing.
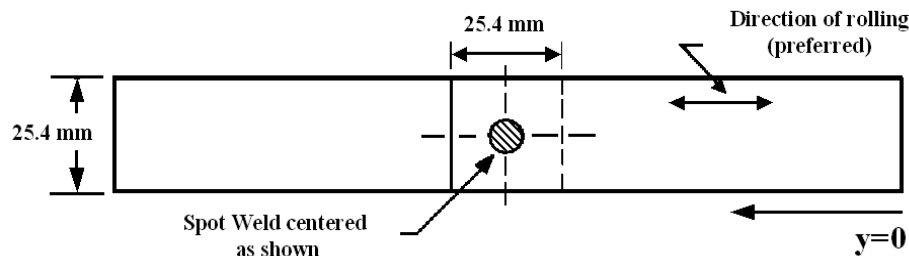

Figure 2b. Schematic diagram of the test specimens subjected to mechanical strength tests.

RESULTS OF THERMOGRAPHIC EVALUATION

The spot-welded plates described in the previous section were evaluated using steady-state IR thermography. A thin coat of flat black paint was applied to the samples to increase their surface emissivity to 0.9. Heat input was provided by four electrical heaters mounted on a copper strip 25.4-mm wide and 3.1-mm thick. The resistors, wired in series, have a total resistance of 200 ohms and a power output of approximately 60 Watts. The heaters were temperature controlled at 71.1°C. The heater strip was mounted on the back side of the steel plate parallel to the lap joint with spring-loaded clamps to ensure good thermal contact (see Figure 3). The heater strip was not mounted directly to the lap joint because, as previously discussed, the sheet metal at the joint is warped by the spot welding process.

Infrared imaging of the spot-welded plates was performed from the side opposite of the heaters so that the spot welds appear as hot spots in the thermograms. The camera used for the experiments is a long-wave (8-12 μm) scanning infrared (IR) imaging radiometer. It has a minimum resolvable temperature difference of less than 0.1°C and an instantaneous field of view of 2 milliradians. The analog images from the camera are digitized, postprocessed and stored on a PC [9]. Images were averaged over 50 frames.

A thermogram of a spot-welded plate with a 50°C temperature range is shown in Figure 4. Light gray corresponds to warm areas and dark gray to cooler areas. The three clamps used to attach the heater strip to the plate are evident at the top of the image. The horizontal line visible in the image below the clamps is the top edge of the lap joint. The strip outlined by the two

vertical lines shows the temperature data plotted in the next section for comparison to data simulated with a thermal model (Figures 11 and 12). Spot welds are not visible because of the large temperature scale used in the image (50°C temperature range).
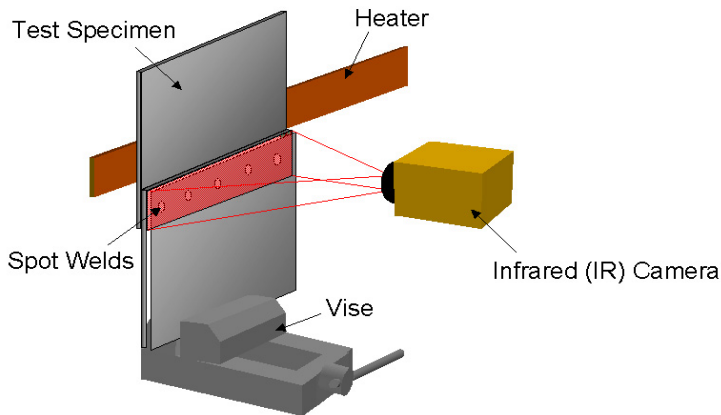

Figure 3. Experimental setup for thermographic imaging.

Plots showing surface temperatures measured along the lap joints are shown in Figure 5. Spot welds with relatively high mechanical strength are easily distinguished from weak welds in the temperature data. The maximum force sustained by each of the welds during mechanical testing is shown in Figure 6.

Figure 7a shows a high-resolution thermogram (5°C temperature range) of the same sample shown in Figure 4. As confirmed by mechanical testing of the spot welds, the joint had two relatively strong welds on the outside edges and three defective welds in the middle. The two strongest spot welds are evident as light spots on the left- and right-hand sides of the image. The surface temperatures measured across the joint along a line running through the welds are plotted in the same figure. The temperature plot shows two well-defined bumps, which are typical spot-weld signatures for relatively strong welds. The thermogram and temperature data displayed in Figure 7b are for a joint with five Type III spot welds. Note the bumps in the temperature plot that correspond to the welds. As discussed in the following section, the temperature gradients around the spot welds can be used to identify defective welds.

POST PROCESSING OF THERMAL IMAGES

A series of post-processing algorithms have been developed to help quantify the data in the thermal images [5]. Unprocessed thermographic temperature data from a lap joint with five spot welds are shown in Figure 8a for a temperature range of 10°C. The two outermost spot welds sustained higher loads during mechanical tests than the middle three welds, which were very weak. The two outer Type III welds appear as light gray areas on the left- and right-hand sides of the

image displayed in Figure 8a. The three defective spot welds in the middle of the joint are not visible in the raw data.

The first step in the post-processing procedure is to remove the temperature gradient in the vertical direction that results from nonuniform heat input due to the location of the heater strip parallel to the lap joint. The raw data is corrected for the gradient by averaging over the pixels in the horizontal direction and subtracting the average from the raw data for that row. Noise is removed from the temperature data using a filtering technique based on convolution of the data with a kernel function as detailed in the reference cited above [5]. In summary, the filtered data are calculated from the inverse Fourier transform of the Fourier product of the thermographic data and the kernel function. The same image displayed in Figure 8a is displayed again in 8b after removing the vertical temperature gradient and filtering the data for noise. Steep temperature gradients are now visible in the regions around the two strongest welds.

Once noise and the vertical temperature gradient have been removed from the data, the data are further processed to obtain temperature gradient images. The value at each pixel in the image is the gradient calculated from the temperatures measured at adjacent pixels in the vertical and horizontal directions. Satisfactory spot welds transmit more heat across the lap joint than defective welds, so there are steep temperature gradients around welds with good weld penetration. The same image displayed in Figure 8b is displayed again in Figure 8c after the additional post-processing described above to obtain a temperature-gradient image. Light-gray areas correspond to small temperature gradients and dark-gray areas to large gradients. The dark areas on the right- and left-hand sides of the image show the steep gradients that occur around relatively strong welds. The three defective welds, which were not visible in the unprocessed image, are now evident as small variations in the heat flow pattern.

The same post-processing was applied to a thermogram of a joint with five Type IV spot welds to obtain the temperature-gradient image displayed in Figure 8d. The steepest temperature gradient corresponds to the darkest region that surrounds the spot weld on the far right-hand side of the image. This weld sustained the highest peak load during mechanical testing of the five welds on the joint. The temperature gradient image obtained for a joint with five defective spot welds is displayed in Figure 8e. The very small gradients around the spot welds are indicative of low mechanical strength. The welds were very weak and broke when the samples were being prepared for mechanical testing.

TABLE 1

SPOT-WELDING PARAMETERS AND TEST RESULTS

	Cycles	Current (Amps)	Average Maximum Load (kN)	Failure Mode
Type I	19	6500	---	10 welds failed before testing*
			2.08	2 welds failed at the weld ("stick" failure)
Type II	14	7800	3.63	stick failure
Type III	14	9100	4.69	stick failure
Type IV	14	10,500	6.24	8 welds: stick failure
			7.24	2 welds: failed at the sheet

* Ten welds failed when the plates were being cut to make the specimens for mechanical testing. The two spot-welded samples that were tested were made from individual steel strips that were not cut from larger plates.

Table 1. Welding parameters and maximum load sustained during mechanical testing.
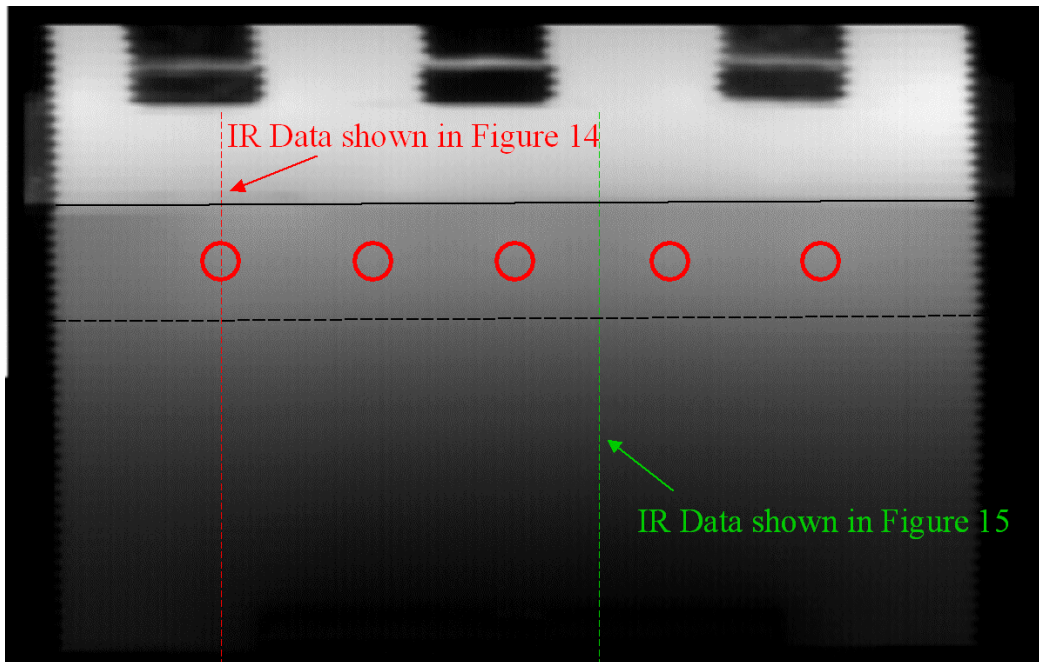

Figure 4. Thermogram of a spot-welded test specimen (Plate 15) for a temperature range of 50°C. The plate had five spot welds at the joint that are not visible in the image because of the large temperature range used in the thermogram. A higher-resolution image (5°C temperature range) is shown in Figure 7a.
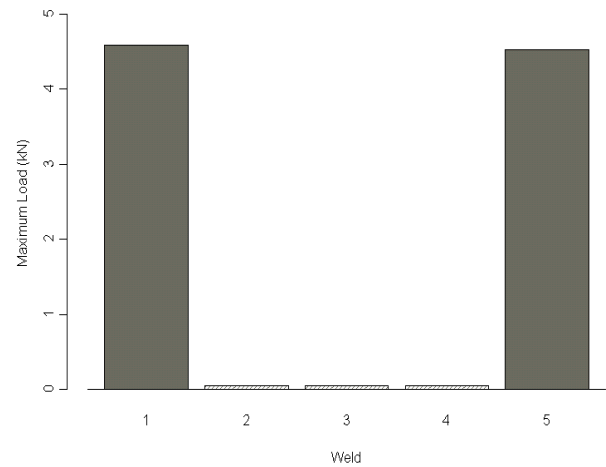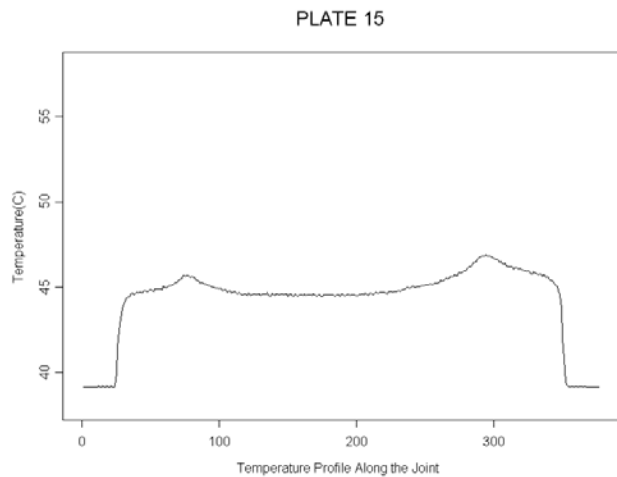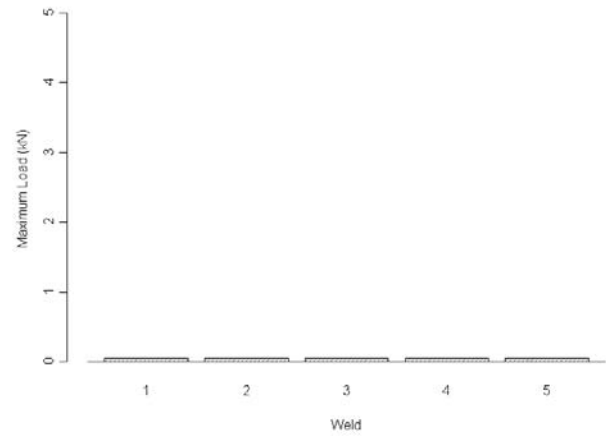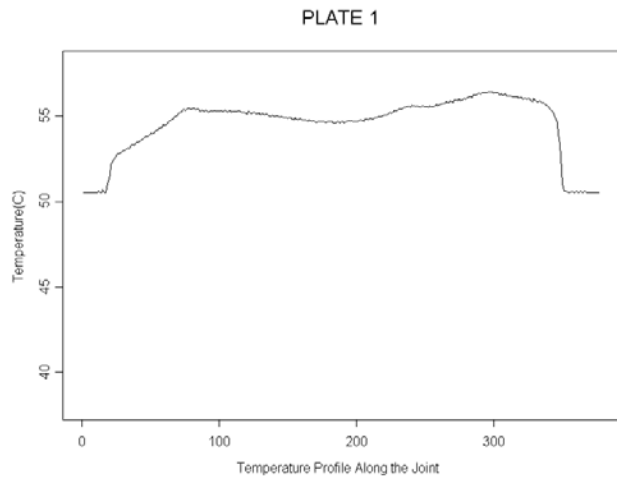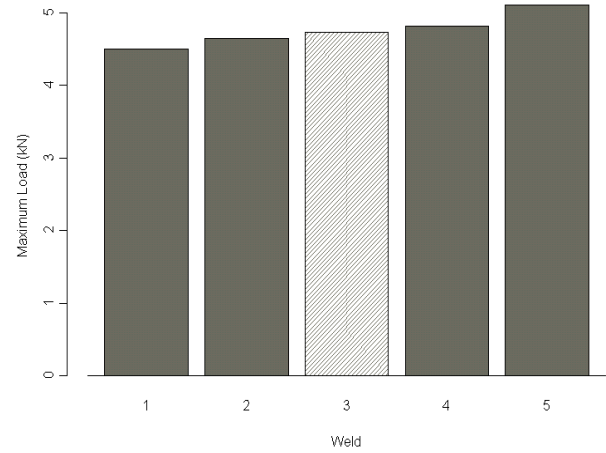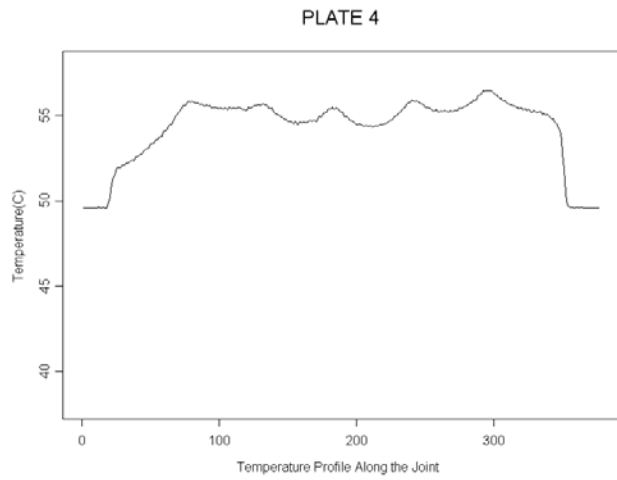
PLATE 4

PLATE 1

PLATE 15

Figure 5. Surface temperatures measured along the lap joints of the plates during thermographic imaging.

Figure 6. Maximum loads attained during mechanical testing of individual spot welds.
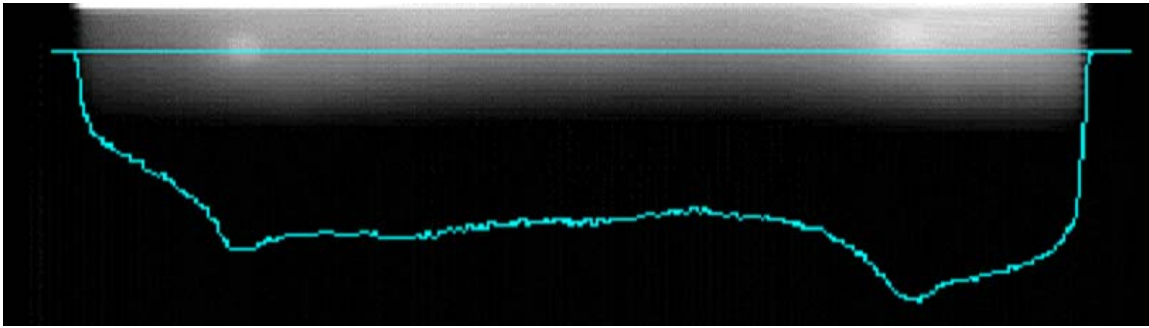
Figure 7a. High-resolution thermographic image (5°C temperature range) of the lap joint on the same test specimen shown in Figure 4. The joint had two Type III spot welds at the outside edges of the plate and three weak, Type I welds in the middle. The stronger welds are visible as bright spots on the left-and right-hand sides of the image. Surface temperatures measured along the joint (on the line indicated) are also plotted.
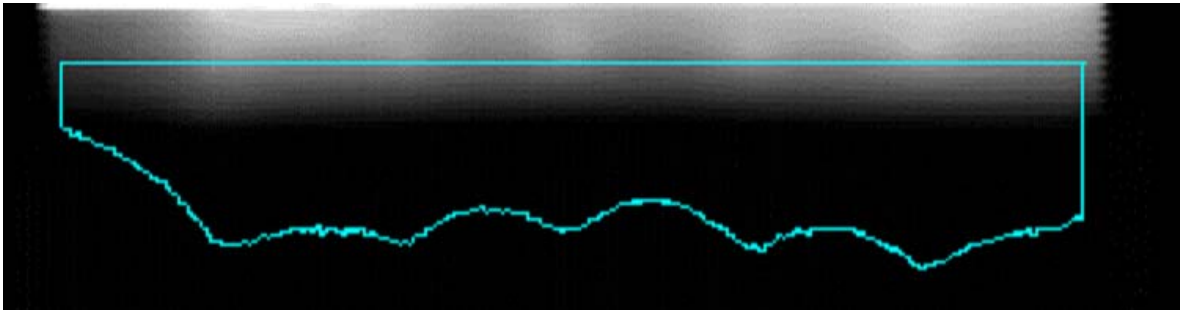

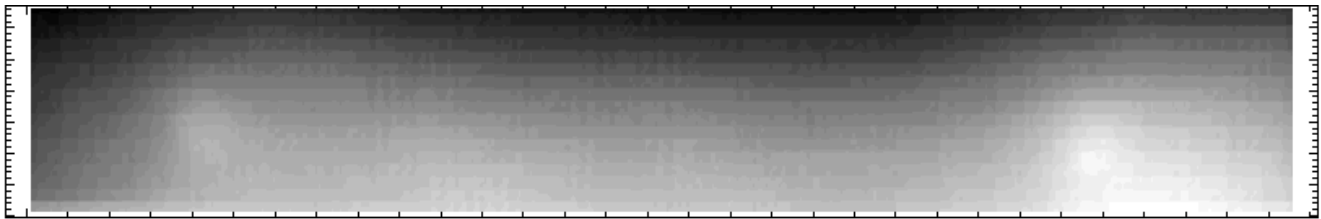Figure 7b. Thermographic image (5°C temperature range) of the lap joint on Plate 4 with five Type III spot welds.

Figure 8a. Unprocessed infrared image with a temperature range of 10°C. Two relatively strong spot welds appear as light areas on the left- and right-hand sides of the image. Three defective spot welds in the middle of the joint are not visible.
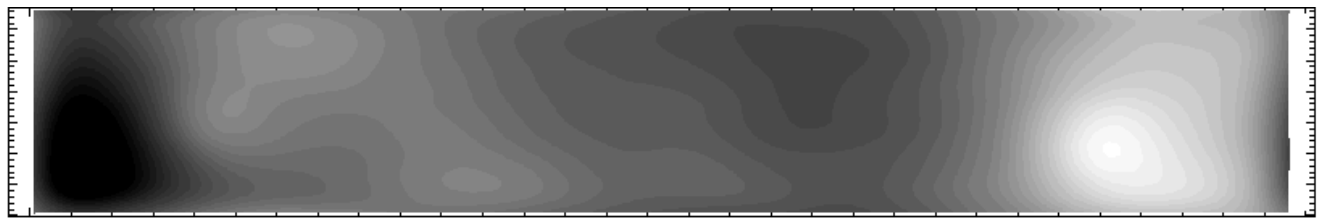
Figure 8b. Same image displayed in 8a after filtering the temperature data for noise and removing the vertical temperature gradient that results from uneven heat input. Steep temperature gradients are visible in the regions around the two strongest welds.
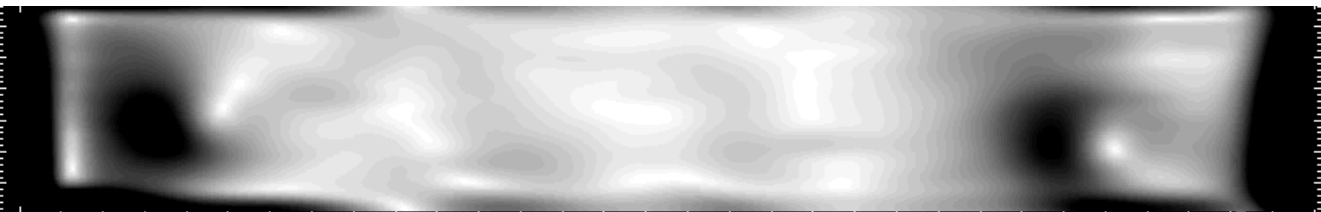
Figure 8c. Same image displayed in 8b after additional post-processing to obtain a temperature gradient image. Light-gray areas correspond to small temperature gradients and dark-gray areas to large gradients. The three defective welds that were not visible in the unprocessed image (8a) are evident in this image as small variations in the heat flow pattern.

Figure 8d. The same post-processing techniques illustrated in 8a-c were applied to a thermogram of a joint with five Type IV spot welds to obtain the temperature gradient image displayed here. The steepest temperature gradient corresponds to the darkest region, which surrounds the spot weld o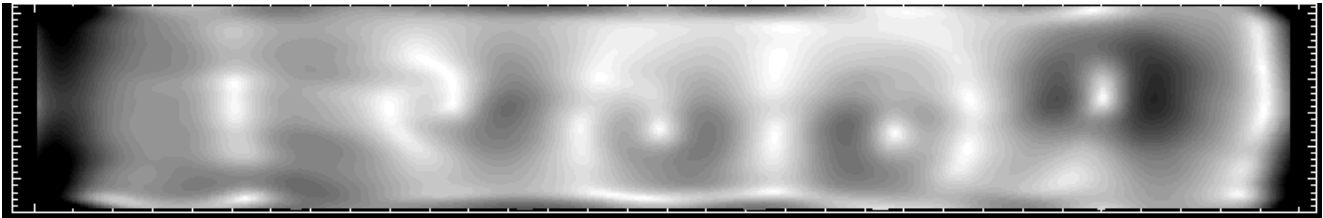n the far right-hand side. During mechanical testing, this weld achieved the highest peak load of the five welds on this plate.
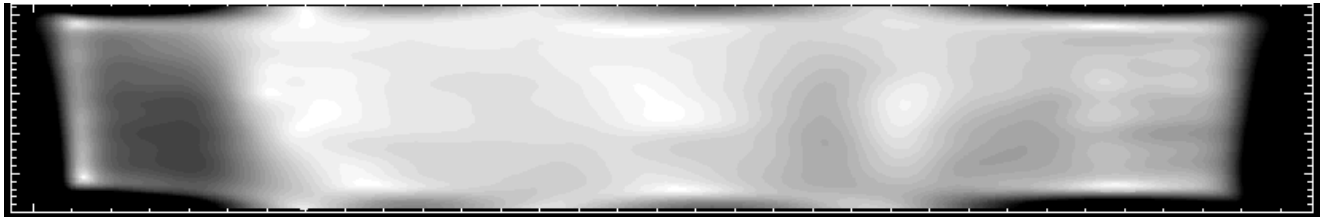

Figure 8e. Temperature-gradient image of a joint with five defective spot welds (compare to Figure 8d). The very small gradients around the spot welds are indicative of low mechanical strength. The welds were very weak and broke when the samples were being prepared for mechanical testing.
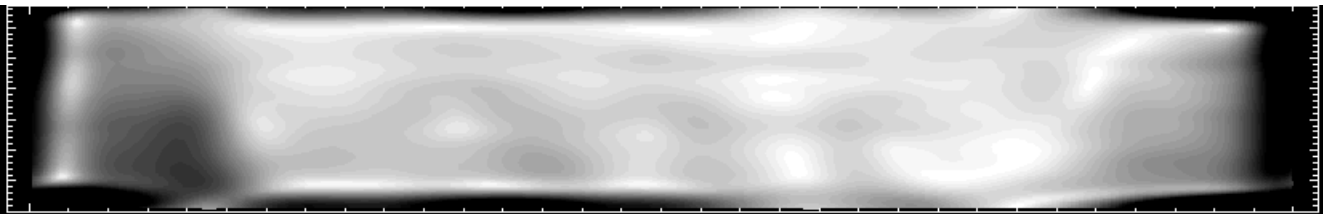

Figure 8f. Temperature-gradient image of a joint with five stick welds (welds with solid but weak contact). Temperature gradients are evident around the welds, but are small compared to those calculated for the stronger spot welds displayed in Figure 8d.

The temperature-gradient image of a joint with five stick welds (welds with solid but weak contact) is displayed in Figure 8f. Temperature gradients are evident around the spot welds, but they are small compared to those calculated for the stronger spot welds displayed in Figure 8d.

Temperature gradients normalized by the ambient room temperature were calculated for the 50 spot welds subjected to mechanical testing. Using a procedure outlined in [5], the maximum difference in the normalized temperature gradient was calculated along a line perpendicular to the joint and running through the center of the weld. The maximum value calculated for each spot weld is plotted in Figure 9 against the maximum force attained during mechanical testing of the weld. The weak spot welds that did not survive sample preparation are plotted at zero force.

The plot shows a strong correspondence between mechanical strength and the temperature gradient calculated from the thermal images of the spot-welded joints. There are two exceptions: in one case a weld with a relatively small temperature gradient sustained a high force, and in another case a very weak weld was associated with a moderately large temperature gradient. The weak weld with a large temperature gradient was near the edge of the plate where a strong

gradient existed because of burs along the edge. Better correlation between the temperature data and strength measurements could be achieved by accounting for temperature gradients in the test specimens that are caused by sources other than the spot welds.

These early results indicate that it may be possible to infer the quality of a spot weld from analysis of the temperature gradients surrounding the welds. Results of thermal modeling presented in the following section indicate that the thermal images have enough resolution to allow the size of spot welds to be determined from the temperature gradients calculated from the images. Assuming that mechanical strength is related to the dimension of the spot-weld nugget, it may be possible to quantify the relationship between thermographic data and mechanical strength.

THERMAL MODELING

Heat transfer through the spot-welded lap joints tested in the laboratory was simulated using a two-dimensional finite-element program called THERM; non-commercial software developed at LBNL and used originally to simulate the thermal performance of glazing components including double-pane windows. The program is well suited to thermal modeling of the lap-joint samples because of its ability to accurately predict heat transfer

Figure 9. Maximum force attained during mechanical testing of individual spot welds versus normalized temperature gradient calculated from the thermograms. Spot welds that broke during sample preparation are plotted at zero force.

across air gaps as well as heat loss due to natural convection and radiation.

The lap-joint samples were modeled using the geometry and dimensions of the laboratory test specimens (see Figure 1). The spot weld was placed in the middle of the joint overlap, and an indentation 0.1-mm deep and 6.0-mm long was used to represent the depression made by the electrodes on the front and back surfaces of the joint. The void space between the plates on either side of the spot weld was modeled as a 0.1-mm-wide air gap. A schematic diagram of the model input to THERM is shown in Figure 10.

THERM has built-in algorithms that calculate an effective thermal conductivity for the air gap taking account of radiation, conduction and convection. The heat input was modeled as a constant heat flux over a distance of 25.4 mm, a distance equal to the width of the heater strip used in the laboratory experiments. For the experiments, the bottom corner of the plate was clamped into a vise over an 11x11 mm² area. The temperature of the vice was approximately 30°C during the experiments, which was incorporated into the model as a constant temperature boundary condition.

SIMULATION RESULTS

Figure 11 shows the results of the simulation of heat transfer across the lap joint through the spot weld. The actual surface temperatures measured by the IR camera in the laboratory are plotted on the same graph. The heat flux used in the model was adjusted through an iterative process until the maximum surface temperature at the center of the heater strip calculated by the model agreed with the temperature measured in the laboratory to within 0.5°C. The room-air boundary condition at the faces of the plates was modeled as a constant surface heat-transfer boundary condition of 8W/m²K. This value is generally accepted for indoor environments. Radiation from the plates to the room was accounted for using a background temperature of 22°C.

The simulated and measured surface temperature curves show excellent agreement. The step in the curves that occurs at 102 mm corresponds to the edge of the lap joint. The measured data shows a smoother transition across the edge than the simulated data because the transient response time of the infrared scanner limits the temperature gradient that can be measured at each pixel. The difference between the simulated and measured data at the upper end of the curves (between 100 and 125 mm) indicates that the location of the heater during the laboratory experiment was slightly higher than that assumed for the simulation. The small discrepancy between the simulated and measured data that occurs between 30 and 75 mm results from use of a constant surface heat-transfer coefficient in the thermal model. In reality, the surface heat-transfer coefficient varies depending on the thickness of the boundary layer of air over the surface created by natural convection.

A second simulation was performed to model the heat transfer across the lap joint outside the area of the spot weld. In this case there is a small air gap between the two plates that was modeled as 0.1-mm wide. The surface temperatures calculated with the thermal model are plotted in Figure 12 along with the temperatures measured in the laboratory. The two curves agree well in shape, but are shifted with respect to one another. Because THERM is a two-dimensional model, the horizontal heat flow that is generated by the spot welds adjacent to the gap is not accounted for. In addition, it appears that the 0.1-mm-gap width used in the thermal model is too wide. These sources of error had much less effect on the first simulation because the heat flux through the spot weld dominates the thermal response.

DATA QUANTIFICATION

An important objective of the thermal modeling work is to help quantify the thermographic data so that it can be used to predict the mechanical strength of welds. The strength of a spot weld is related to the size of the weld

nugget and weld penetration. A series of simulations were performed to determine if the thermographic imaging techniques described in the previous section had the resolution required to discriminate between spot welds of different size. Simulations were run for weld nugget diameters of one, two, four, and six mm. All other dimensions and parameters were the same as for the simulations described in the previous section.
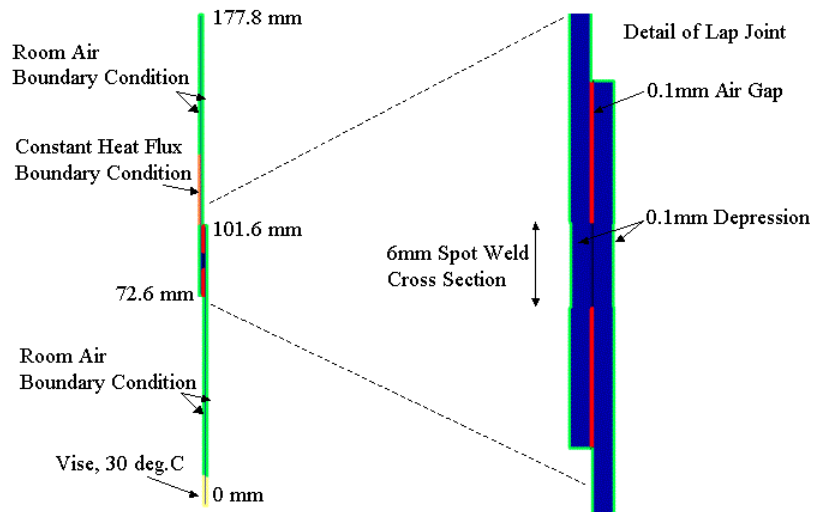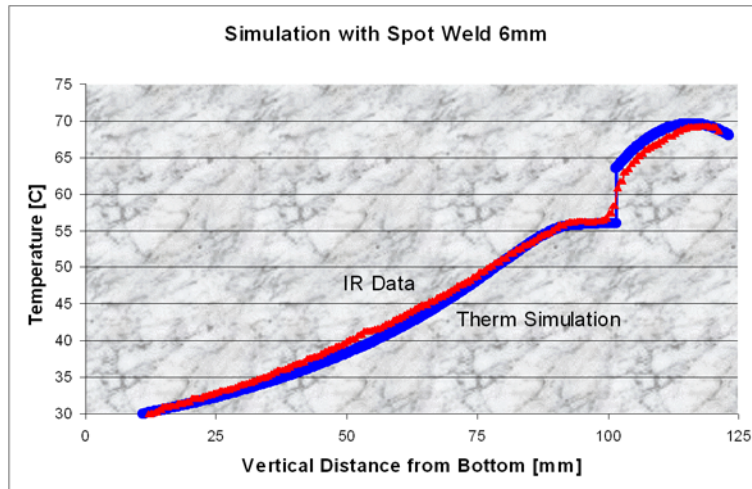

Figure 10. Geometry of lap-joint samples and boundary conditions used for thermal modeling.

Figure 11. Comparison between simulated and measured surface temperatures across a lap joint through a 6-mm-diameter spot weld.
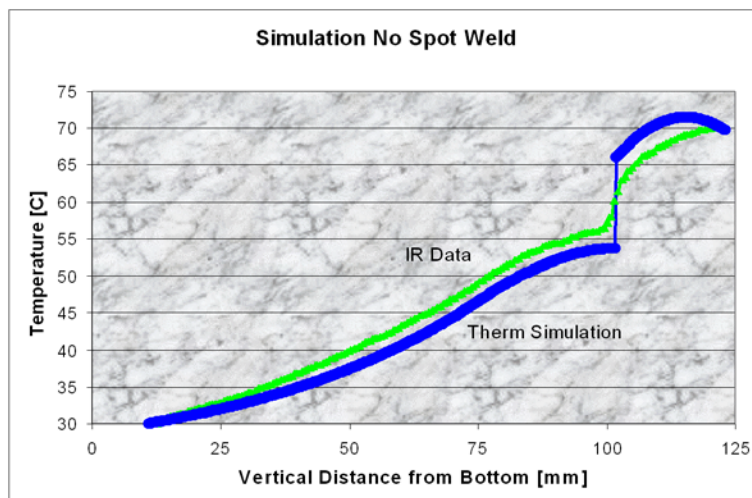
Figure 12. Comparison between simulated and measured surface temperatures across a lap joint adjacent to a spot weld.
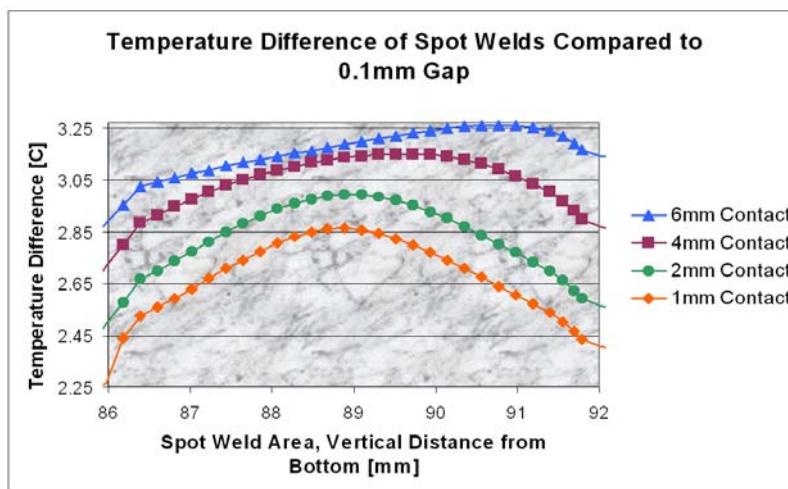
Figure 13. Differences in surface temperatures across a lap joint through spot welds of different diameter calculated with the thermal model. The temperatures calculated adjacent to the spot weld (assuming a 0.1-mm-air gap between plates at the joint) were subtracted from the temperatures calculated at the spot welds and the differences are plotted.

Surface temperatures were calculated with the thermal model along lines perpendicular to the lap joint through the centers of the spot welds. To highlight the effect of the spot welds, the temperatures calculated along a line across the joint between welds (assuming a 0.1-mm gap between the plates) were subtracted from the corresponding temperature data for the spot welds. The resulting temperature differences are plotted in Figure 13 for the four spot-weld diameters. The four curves are clearly distinct. The simulation data suggests that an IR camera with 100 mK thermal resolution should be able to differentiate between spot welds with different diameter weld nuggets.

PULSE THERMOGRAPHY OF RESISTANCE SPOT WELDS IN GALVANIZED STEEL

In contrast to the samples used in the previous sections (described in Figure 2), the test specimens used for the experiments described here were made with spot welds in galvanized steel sheets. During welding, expulsion of the zinc coating creates a weak solder joint around the weld nugget. Although structurally weak, the zinc bond is an area of solid thermal contact that is difficult to distinguish from the weld nugget. The indentation of the surface caused by the welding electrodes also complicates measurements, because it changes the travel time of the thermal pulse through the specimen in the vicinity of the weld. Despite these problems, preliminary work indicates that pulse thermography is capable of identifying some weld characteristics, even in galvanized steel.

Several post-processing techniques have been applied to thermographic images of spot welds to help determine the feasibility of using thermography to nondestructively evaluate the size of weld nuggets. Results are summarized in Table 2.

POST-PROCESSING TECHNIQUES

Maximum contrast of time-series data based on temperature gradients

The maximum-contrast image displays data captured after the heat pulse has traveled through the specimen, at the point where the temperature difference between the steel sheet and the spot weld is at its maximum value. Lateral heat flow blurs the spot weld in the thermal images as soon as a temperature difference develops. Shortly before the maximum temperature contrast occurs, the spot weld is visible in the image with the sharpest boundary definition observable. This frame can be found by systematically going through temperature-gradient images (see below for a description of the temperature-gradient image). The surface-temperature frame where the maximum gradient occurs is shown in row 1 of Table 2.

Smoothed, 3D, maximum-contrast image

The processing described in this section is very sensitive to noise. Noise in the temperature data is induced through many different mechanisms. The most significant sources include: random photon emission and detection, spontaneous electron emission of the detector (dark current), amplification noise, and analog-to-digital conversion. An Epanechnikov smoothing function is applied to each frame. This function calculates a weighted temperature average of the surrounding pixels for each pixel of the frame. The number of pixels included in the smoothing process is user defined. A compromise between sufficiently smooth data and adequate representation of the features of interest needs to be accomplished. Too much smoothing blurs the contrast; too little smoothing will cause grainy images or, in the worst case, will result in useless post-processed data. The images in this row of the table were obtained by smoothing the data from the previous row, and displaying the data in a three-dimensional representation with identical color coding.
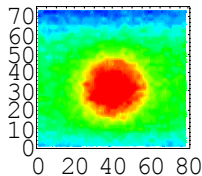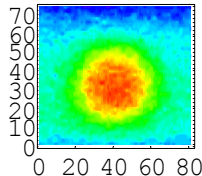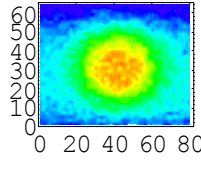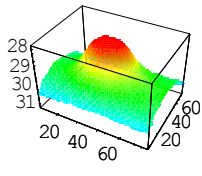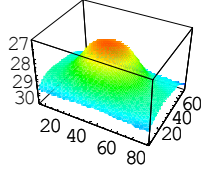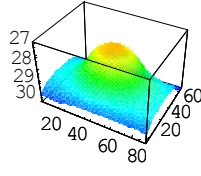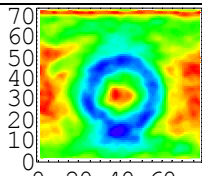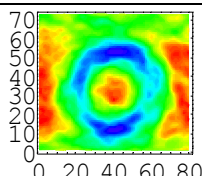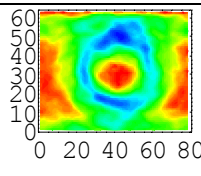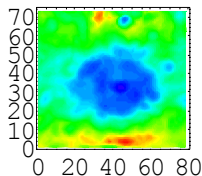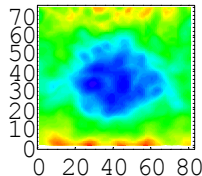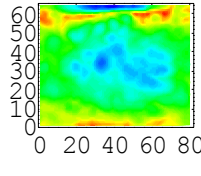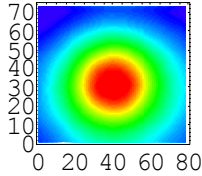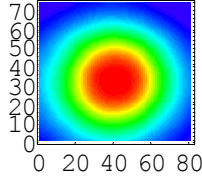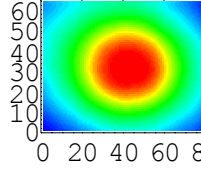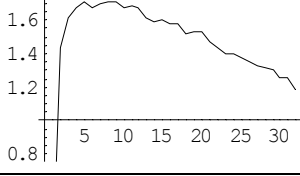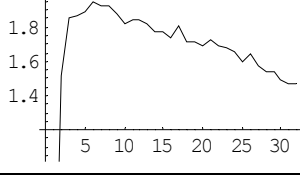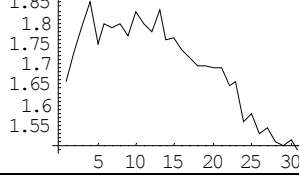
Technique	Sample 1 Good spot weld	Sample 2 Undersized spot weld	Sample 3 Stick weld
Maximum contrast of time-series data based on temperature gradient			
Smoothed, 3D, maximum contrast image			
Temperature-gradient image of maximum-contrast data			
Maximum-phase image			
Maximum-amplitude image			
Temperature difference evolution between weld and sheet			
Maximum Gradient	0.13488	0.134398	0.153436

Table 2. Different post-processing techniques are illustrated for thermal images of a satisfactory, undersized, and stick weld.

Temperature-gradient image of maximum-contrast data

The temperature-gradient image is calculated from the smoothed data, and represents the first temperature derivative in two dimensions (for each frame). Numerically, the derivative is calculated as the difference between the original frame, and a frame where the data was shifted to the right and down by one pixel. The final result is the square root of the sum of the squared differences. Because this method is based on a spatial pixel-to-pixel difference, one row and one column of data are lost.

Pulse-Phase Thermography (PPT) combines modulated thermography, in which test specimens are thermally stimulated with one frequency and amplitude, with pulsed thermography. The thermal pulse applied to the part is assumed to have a rectangular time characteristic with a uniform intensity for the entire duration of the pulse. This pulse can be interpreted as a broad band of frequencies and amplitudes being launched into the part. The smoothed temperature data are used to calculate the Discrete Fourier Transform for each pixel in the time series. The Fourier transform returns two values for each pixel of the frame, a real and an imaginary number. Successful implementation of this technique requires attention to the frame rate and the number of frames acquired. Fast Fourier Transforms (FFTs) work best on data sets with frame numbers equal to a power of two, but this is not a requirement. For instance, 32 or 64 frames acquired without time delay, starting immediately after the thermal pulse. Frequency resolution depends on the length of the acquisition time. Acquisition times that are too short cut out low frequencies, possibly causing the loss of valuable information. The IR camera

physically limits the maximum frame rate, and therefore the sampling rate. Aliasing errors are introduced if the signal bandwidth exceeds the sampling bandwidth (i.e., under sampling).

Maximum-phase image

The phase is defined as $\phi(u)=\tan^{-1}(Im(u)/Re(u))$ of the FFT. The maximum-phase image is based on the maximum-phase value for each individual pixel in space. In general, maximum-phase images can more accurately visualize defects at depth with clearer defect contours than maximum-contrast images. In the case of spot welds, the maximum phase image appears to be a good indicator of how well the two sheets are connected. Cold welds exhibit a different phase behavior because part of the thermal energy is reflected at the sheet interface instead of traveling all the way through the nugget. This behavior can also be seen in the maximum-contrast images, where the maximum contrast occurs earlier for a cold weld than a good weld.

Maximum-amplitude image

The amplitude is calculated as $I(u)=Sqrt(Im(u)^2+Re(u)^2)$. Analogous to the calculation of maximum phase, the maximum amplitude is calculated for each spatial pixel. For spot-weld analyses, this technique does not appear to return any valuable information.

Summary

Initial results indicate that maximum-contrast images can be an indicator of spot-weld size, but are not reliable in distinguishing cold welds from good welds. Zinc solder zones are also visible, and in the case of cold welds, also contribute to the overall apparent size. Temperature-gradient images can be used to evaluate spot-weld quality in uncoated steel sheets. The zinc solder zone also causes strong temperature gradients, making it impossible to use gradient magnitude as an indicator of weld quality. It appears that good welds have smaller outlines in the gradient image than undersized and cold welds. This could be caused by higher temperatures present during welding, which burn away the zinc in close proximity of the nugget. The maximum-phase images appear to be a reliable indicator for cold welds. In this case, part of the thermal energy is reflected at the sheet boundary leading to a difference in the phase response. With the different processing techniques outlined here it is possible to evaluate spot-weld quality based on information obtained for a good weld, which is used to set processing parameters. Distinguishing stick welds from solid nuggets appears to be feasible, but determining the exact weld nugget diameter to classify good from undersized welds is not possible with the techniques presented here. The effect of the electrode indentation still needs to be analyzed. In addition, thermal diffusivity measurements on plain sheets and nugget material would provide useful information that could be used to optimize pulsed-thermography parameters and post-processing routines.

ACOUSTIC METHODS

Acoustic methods used to detect and characterize defects in joints can be roughly classified according to the frequency of the waves used. Detection resolution increases with frequency, while spatial resolution generally improves with the number of measurements made on the sample. High-frequency techniques provide good spatial resolution of defects, but usually require time-intensive scanning of the joint. In contrast, methods employing resonance of the structure require limited measurements of the frequency response function, but are not capable of locating defects without some form of back-analysis of the measurements. Techniques based on selective probing of the structure are a promising alternative if some level of defect characterization can be achieved within assembly-line time constraints.

The criterion commonly used in industry to characterize the quality of spot welds is based on the size of the weld nugget measured after peeling the spot-welded joint. A weld is judged to be satisfactory if the diameter of the nugget is greater than $4\sqrt{t}$, where t is the thickness of the sheets. To achieve a dimensional characterization of the weld nugget using a nondestructive ultrasonic technique requires using a relatively high-frequency method. Acoustic microscopy is one such method, allowing measurement of the physical dimensions of defects by scanning an acoustic beam over the area containing the defect. Although this method is not practical for inspection in a production environment, it is useful in determining the sensitivity of other acoustic techniques to structural changes in the weld nugget usually associated with the welding process. In addition, acoustic microscopy is very valuable in helping to evaluate emerging phased-array technologies, which may be practical for use in manufacturing plants. Phased-array systems under development allow focusing and steering of acoustic waves, and should be able to perform the same kind of inspection that is possible using acoustic microscopy.

ACOUSTIC MICROSCOPY

Acoustic microscopy is almost identical in principle to that of reflection seismology. Acoustic waves are propagated into the sample, and images of surfaces and microstructures are obtained based on reflected waves measured at the surface [10]. Reflections occur when there are changes in impedance in the sample, for example, at interfaces, cracks, and voids, or when there is a change in material properties. Return echoes are proportional to the change in impedance in the material. The return times are a function of the distance from the interface to the receiver. By scanning over a sample and analyzing the positions in time and space of the echoes, it is possible to determine the position and the depth of defects or interfaces present in the sample [11].

Samples used for the acoustic microscopy experiments were different than those described above that were used for the thermographic measurements. For the

results presented in this section, the test specimen was a stainless-steel strip with five welds. The quality of the welds was varied by changing the level of current used during welding. No adhesive was applied to the joints. The thickness of the individual sheets was 1.65 mm. The surfaces of the sample were polished because of the sensitivity of the method to surface conditions.

The experiments were performed with the transducer focused at the interface between the two sheets to magnify the amplitude of the reflection off this interface. For each position of the focused probe in the X-Y plane, an A-Scan was recorded, which is a plot of amplitude versus time. An electronic gate is positioned in time, and controlled to open for a defined duration, allowing only the information from a specific depth to be recorded. The inspection depth was located at the interface between the steel sheets, so the electronic gate was set to capture only the reflection coming from this interface. The samples were scanned in a water tank, to ensure good coupling between the acoustic transducer and the test specimens.

The images displayed in Figure 14 are C-Scans, obtained using a transducer working at the central frequency of 50 MHz. A C-Scan provides a two-dimensional image of echoes arising from reflections at a particular depth in the sample, in this case, reflections off the interface between the two sheets. Measurements were made on a grid with 0.25-mm spacing. Dark gray corresponds to areas where reflections have relatively low amplitude compared to areas with high-amplitude reflections, shown in light gray. In the area of the weld nugget where the steel sheets are fused together, only small-amplitude reflections are observed, which indicates that the acoustic waves are being transmitted through the weld into the lower sheet. Outside of the fused zone, the interface between the sheets generates high-amplitude reflections because of the large impedance difference between steel and water (since the sample is immersed, water infiltrates the interface between welds). As discussed previously, the steel sheets deform during the spot-welding process (see Figure 2). Even in the case of minimal deformation (Figure 2.e), the contact between the two sheets in the immediate vicinity of the welds is not sufficient to allow transmission of high-frequency acoustic waves.

Experiments performed to date indicate that the diameter of the low-amplitude zone visible in the images displayed in Figure 14 is directly proportional to the diameter of the weld nuggets measured when the samples are peeled. The measured nugget diameters vary from 5 to 7.5 mm. Using the $4\sqrt{t}$ size criterion defined previously, the last three spot welds on the right-hand side in Figure 14 would be judged satisfactory, and the two others would be labeled "undersized." These results are in accordance with the welding parameters used to make the welds. Work underway is focused on quantifying the relationship between the low-amplitude fused zone and the size of the weld nugget measured when the joint is peeled open.

It is also possible to detect delaminations, cracks, and other anomalies using acoustic microscopy. A close-up image of the nugget zone in the third spot weld (Figure 15) shows a crest in the center of the nugget (indicated by the white circle). The crest is a reflection caused by a change in impedance, which may indicate the presence of a void or a crack. Such changes in amplitude are visible in the center of all five welds. This may indicate the existence of porosity in the weld nuggets.
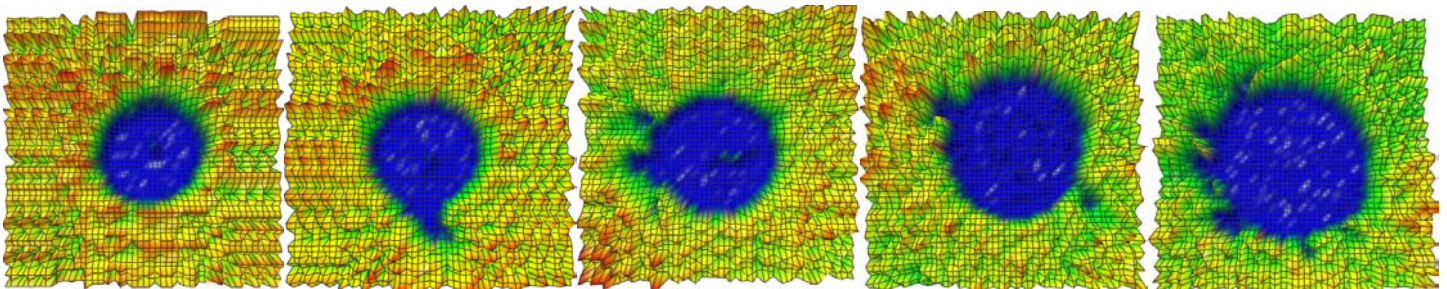

Figure 14: C-Scan images of spot welds made using acoustic microscopy. The quality of the welds varies from undersized (left-hand images) to satisfactory (right-hand images).
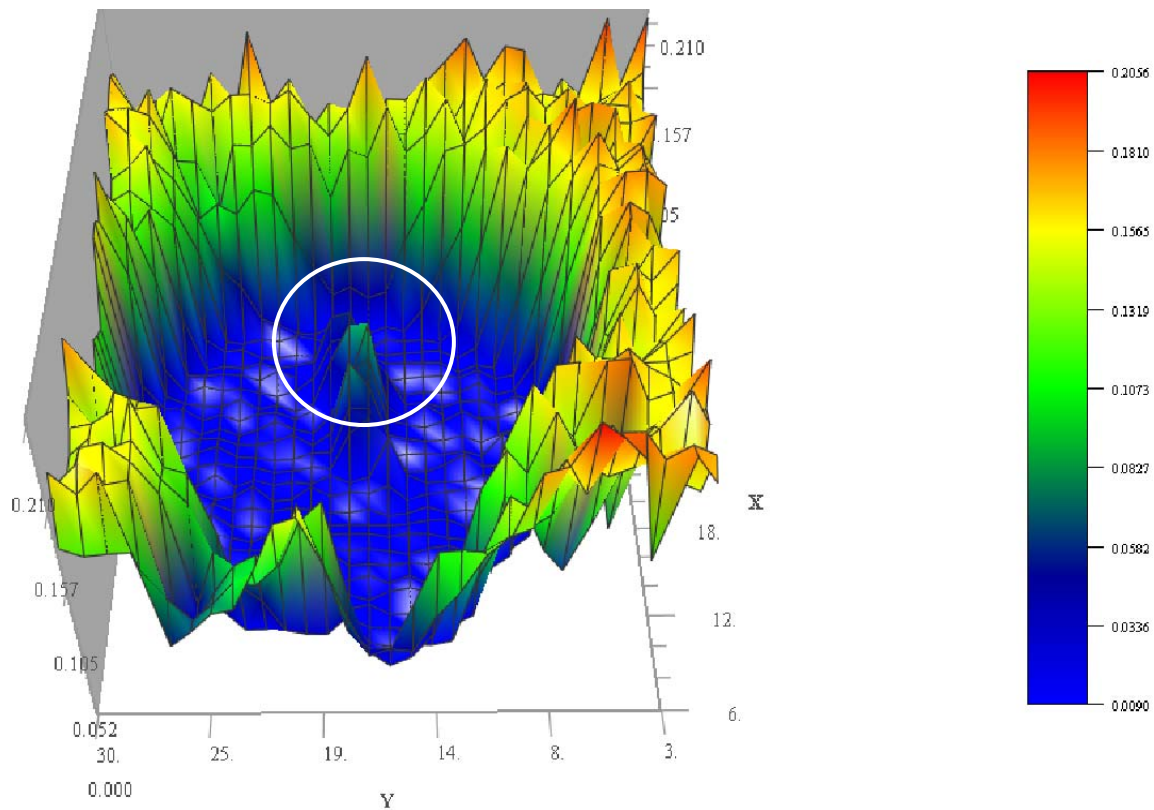
Figure 15: Close-up view of the nugget zone in the C-Scan image obtained for the third weld in Figure 14. The white circle indicates reflections coming from the middle of the weld nugget, suggesting the existence of a defect inside the weld.

It is important to keep in mind that these experiments were performed on uncoated stainless-steel samples. As discussed previously, for galvanized steels, the melting point of the zinc coating is usually lower than that of the steel. During welding, the coating melts, creating a weak bond between the sheets that may conduct acoustic energy. Using acoustic microscopy to measure the diameter of the weld nugget depends on there being no energy reflected back to the transducer in the weld-nugget zone; i.e., it is assumed that in the area of the nugget, the acoustic waves propagate through both sheets without being reflected. If a weak zinc bond forms during welding that allows transmission of the acoustic waves into the lower sheet, then the estimated nugget diameter will be too large, resulting in undersized welds being judged satisfactory. This is not a problem if there is a sufficient difference in impedance between the coating and the steel to cause a reflection off the zinc bond. It is difficult to design experiments to examine the acoustic behavior of these weak zinc bonds because of the difficulty of polishing the samples without breaking the bond. However, as discussed in the following section, a finite-difference model has been developed to help resolve this issue, and better understand the propagation of acoustic waves in spot-welded joints.

FINITE-DIFFERENCE MODELING

Modeling ultrasound propagation in welded parts is a valuable tool for helping to develop inspection strategies and interpret laboratory results. While the base material can be considered isotropic and homogeneous ferritic steel, anisotropy and heterogeneity should be taken into account in the fused zone described as the weld nugget. The grain structure in the nugget takes on a cast-like columnar or austenitic structure, which is considerably coarser than the grain structure in the base material [12]. This difference in microstructure is the basis for many commercial ultrasonic inspection systems, as discussed previously. A finite-difference scheme has been developed to study the propagation of ultrasonic waves in anisotropic and viscoelastic materials. An advantage of finite-difference techniques is that it is relatively easy to define complicated boundaries and shapes to model defects such as inclusions. A staggered grid is used that yields second-order accuracy in time and fourth-order accuracy in space [13]. The viscoelastic behavior is represented by an anelastic tensor [14, 15]. This formulation allows different attenuations to be specified for different directions of propagation. Figure 16 shows a micrograph of a spot weld containing inclusions, and a snapshot in time obtained from the finite-difference model. The dark lines in the snapshot represent acoustic waves propagating through the sample. The image shows how the waves are reflected and diffracted off various features such as inclusions and the interface between the two sheets.
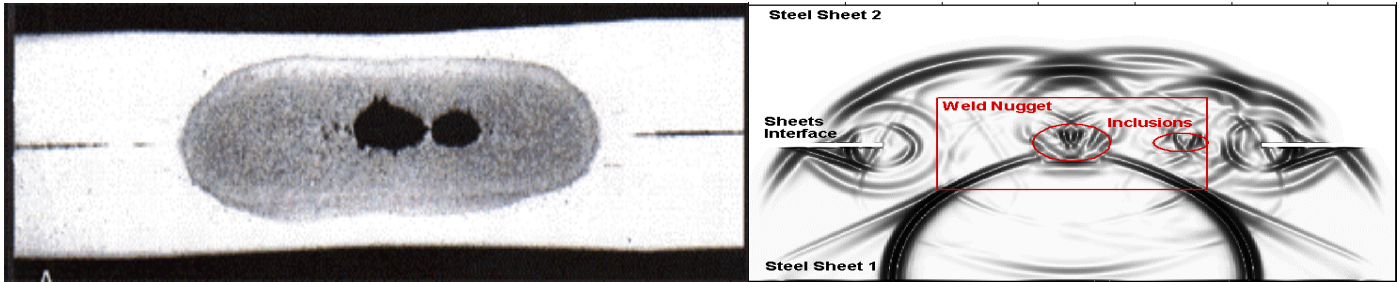
Figure 16: Micrograph of a spot weld containing inclusions (left-hand image) and snapshot of acoustic waves propagating into a spot weld (right-hand image). The rectangular region in the center of the model (right-hand figure) is the weld nugget; the elliptical features in the rectangle represent the inclusions.
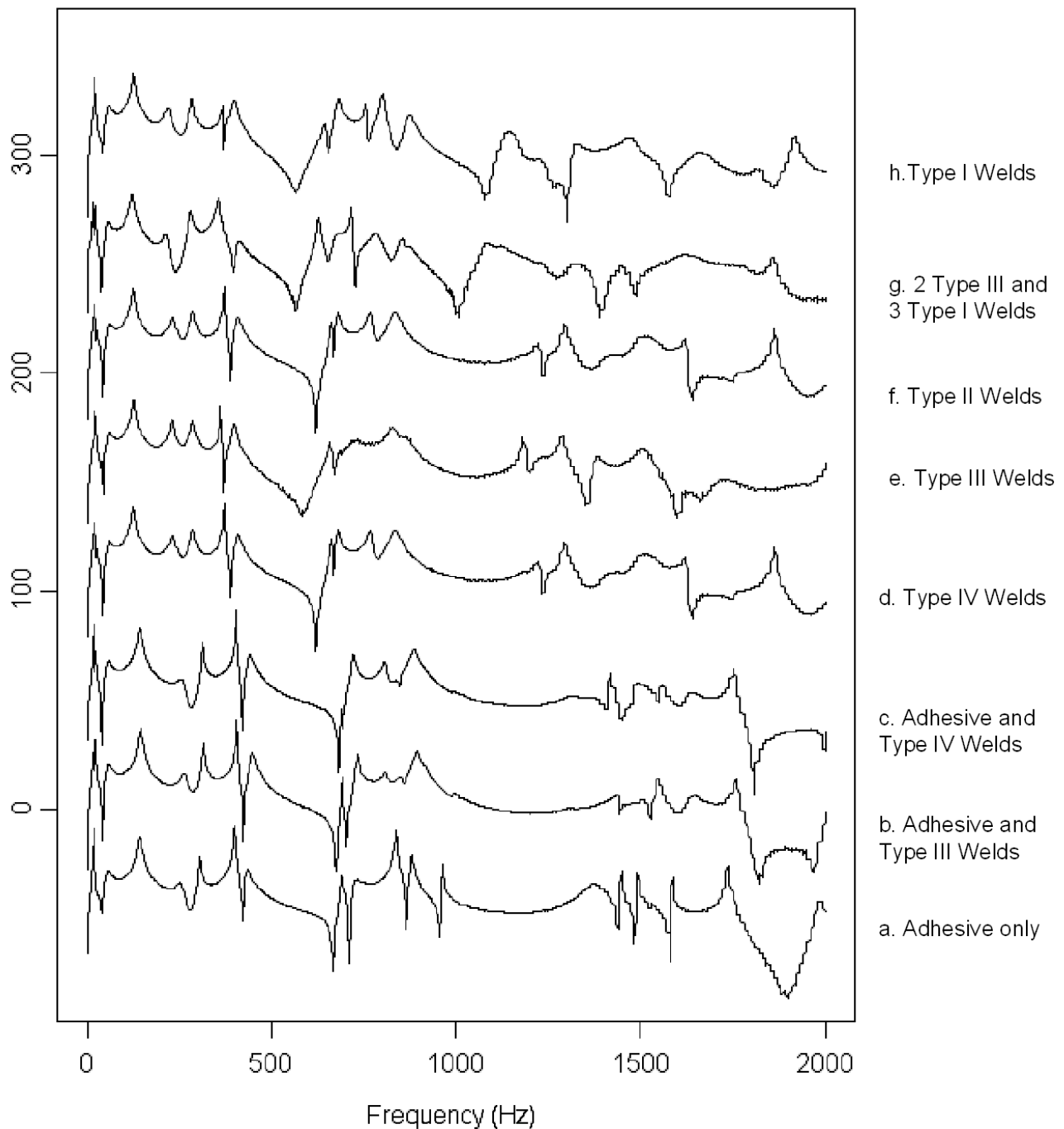

Figure 17. Spectral response of lap-joint test specimens excited with a mechanical shaker.

GLOBAL RESONANCE TECHNIQUE

For assembly-line inspection, where both time and access to joints is extremely limited, global resonance methods hold promise because they are fast, robust, and require a minimal number of sensors and measurements. Resonance techniques are particularly attractive for inspection of joints because of their sensitivity to joint and structural stiffness.

The results of global resonance tests are shown in Figure 17 for steel plates joined with a single lap joint. The test specimens had the same geometry and dimensions as shown in Figure 2a. Tests were performed on samples with spot-welded joints with and without adhesive, and one sample with an adhesive-bonded joint with no spot welds. The test specimens included the plates previously discussed with respect to thermographic analysis of individual spot welds (Plates 1, 4, and 15). For the resonance measurements presented here, the steel plates were clamped into a vise and excited by a mechanical shaker. The input to the shaker was a 0-50 kHz pseudo-random signal. The global spectral response was measured at the top right-hand corner of the plates using a noncontact laser-Doppler vibrometer.

Perhaps the easiest thing to see in the figure is that there are substantial differences between the spectra for three general groups: the adhesive-bonded joints with and without spot welds (17a-c); the spot-welded joints with Type II, III, and IV welds (17c-f); and the spot-welded joints with three or more fragile Type I welds (17g-h). These differences in spectra are easiest to see in the frequency range between 500 and 1500 Hz. Comparing the spectra at frequencies between 100 and 500 Hz it is possible to see that the resonance peaks for the adhesive-bonded and weld-bonded joints (17a-c) are shifted upward with respect to the peaks for the spot-welded joints (17d-h), reflecting the higher stiffness of the adhesive-bonded joints. It is also possible to see differences between the spectra for the weld-bonded joints (17b and 17c) and the adhesive-bonded joint (17a), particularly for the frequency band between 600 and 1600 Hz.

These initial results indicate that spot-welded joints with fragile welds are easily distinguishable from joints with stronger welds, even for the case where three fragile welds are surrounded by two stronger welds. The spectra for the joints with adhesive are easily distinguished from the spot-welded joints with no adhesive. Furthermore, the spectra for the weld-bonded plates are different from the spectrum for the adhesive-bonded plate with no spot welds. The spectra for the spot-welded plates with welds of Types II, III and IV (17d-f) are similar, and additional experiments are necessary to determine if global resonance techniques can effectively discriminate between welds of these three types.

TECHNICAL SUMMARY

In general, infrared thermography has the advantages of being a fast, full-field imaging technique applicable to a wide range of materials. For manufacturing applications, adequate accessibility to parts may be a problem, as well as requirements that parts be clean and have a high surface emittance. Heat input is also an issue, particularly for complicated three-dimensional structures. The viability of thermography for manufacturing applications can be improved by development of three-dimensional heat-flow models to characterize thermal response, fast data-processing algorithms, and image-enhancement software.

Thermographic imaging techniques were successfully used to evaluate individual spot welds. Initial results obtained using post-processing algorithms developed to analyze thermal images of spot-welded joints indicate that the quality of a spot weld can be inferred from analysis of the temperature gradients surrounding the weld. As the first step in developing algorithms to perform quantitative analysis of thermographic images, a thermal model was developed for the spot-welded plates tested in the laboratory. Results of the thermal modeling indicate that it should also be possible to determine the size of spot welds from analysis of the thermal gradients in thermographic images. To the degree that mechanical strength is related to the dimension of the spot-weld nugget, it should be possible to relate thermographic data to mechanical strength.

Analyzing the exact size of the nugget in a resistance spot weld is feasible with steady-state and pulsed thermography for plain uncoated steel or stainless steel sheets. For galvanized steel, solder zones surrounding the spot welds form a solid bond that is difficult to distinguish from the nugget. Maximum-phase images are able to identify stick welds because the thermal wave is partially reflected at the interface between the sheets. Pulse-phase thermography can contribute to characterizing laboratory calibration samples, which, in turn, can be used to evaluate different NDE techniques. To improve post-processing techniques, more research is required to determine the influence of the surface indentations caused by the welding electrodes on the propagation of thermal waves.

Acoustic microscopy was successfully used to evaluate welds in stainless-steel samples. The method allows measurement of the weld-nugget diameter, which is the criterion chosen by industry experts as being the most reliable in determining the quality of the weld. Acoustic microscopy can also identify defects such as porosity or cracks in the weld nugget. Additional work is required to determine if the technique can successfully identify the weld nugget for welds in galvanized steel. Being able to determine the weld-nugget diameter nondestructively would allow fabrication and testing of specimens that could be used to calibrate and evaluate other NDE methods without destroying the sample. Understanding acoustic microscopy results also helps in designing and

characterizating new ultrasonic inspection techniques such as phased-array technologies. Phased-array sensors are an emerging technology that allow focusing and steering of acoustic beams, and hold the promise of allowing nondestructive dimensional inspection of welds.

Global resonance techniques are particularly attractive for online inspection because they are fast, robust, and require only limited access to the part or structure being tested. Although not well suited to the inspection of individual spot welds, the method may prove valuable for testing joints and large spot-welded structures because of its sensitivity to structural stiffness.

CONCLUSIONS

Work to date demonstrates that characterization of individual spot welds is possible using thermographic imaging techniques and acoustic microscopy. Research issues include determining the sensitivity of the methods to surface roughness and the indentation of the surface caused by the welding electrodes. Welds in galvanized steel are more difficult to inspect because expulsion of the zinc coating during welding creates a weak solder joint around the weld. Global resonance techniques are sensitive to structural stiffness, and were successfully used to identify joints with weak welds, and to distinguish between joints with and without adhesive.

Stick welds, characterized by solid but weak contact, can be difficult to detect using conventional nondestructive methods in part because of deformation of the lap joint that occurs during formation of the weld. The spot-welding process deforms the joint surfaces creating gaps at the interface between the metal plates in the areas surrounding the welds. It is possible, therefore, to have greater overall contact area across joints formed with weak welds than across joints with strong welds. As a result, caution must be exercised when interpreting acoustic and thermographic data because joints with very weak spot welds can conduct heat and acoustic energy as well or better than joints with stronger welds. Nonetheless, acoustic and thermographic scanning techniques and global resonance data were successfully used to identify stick welds on spot-welded and weldbonded joints.

For those acoustic and thermographic methods that prove feasible for online inspection, the remaining research challenge is to develop, test, and refine the techniques so that they are suitable for large-scale manufacturing applications. This requires sensor development, integrated real-time diagnostic tools that operate at sufficient speed for assembly-line use, determination of resolution limits and the best diagnostic parameters for specific applications, and demonstration of robustness, accuracy, and cost-effectiveness under realistic operating conditions.

REFERENCES

1. American Welding Society, 1997. Recommended Practices for Test Methods for Evaluating the Resistance Spot Welding Behavior of Automotive Sheet Steel Materials, *Specifications Standards and Codes from the American Welding Society.*
2. N. Guillaume, D. Hopkins, S. Nakagawa, and K. Nihei, 2000. Complications of Using Resonance-Frequency Shifts to Detect Defective Joints, *Review of Progress in Quantitative Nondestructive Evaluation,* Vol 19, D. O. Thompson and D. E. Chimenti (eds.), pp. 1285-1293.
3. K. Nihei, S. Nakagawa and D. Hopkins, 1999. Defect Detection Using the Reverberant Wavefield, *Review of Progress in Quantitative Nondestructive Evaluation,* Vol. 18, D. O. Thompson and D. E. Chimenti (eds), pp. 1517-1523.
4. D. Türler, D. Hopkins, S. Nakagawa, A. Valente, and K. Nihei, 1999. Thermographic and Acoustic Imaging of Spot-Welded and Weld-Bonded Joints, *Review of Progress in Quantitative Nondestructive Evaluation,* Vol. 18, D. O. Thompson and D. E. Chimenti (eds.), pp. 1543-1551.
5. D. Hopkins, S. Nakagawa, K. Nihei and D. Türler, 1998. Imaging Flaws in Adhesive Joints Using Acoustic Techniques and Infrared Thermography, *Review of Progress in Quantitative Nondestructive Evaluation,* Vol. 17, D. O. Thompson & D. E. Chimenti (eds.), New York: Plenum Press, pp. 1387-1394.
6. T.M. Mansour, 1988. Ultrasonic Inspection of Spot Welds in Thin-Gage Steel, *Materials Evaluation,* Vol. 46, pp. 650-658.
7. D. Türler, 1999. Predicting the Geometry and Location of Defects in Adhesive and Spot-Welded Lap Joints Using Steady-State Thermographic Techniques, in *Proc. of SPIE the International Society for Optical Engineering,* Vol. 3700, Dennis H. LeMieux and John R. Snell Jr. (eds.).
8. M. Balesand and C. Bishop, 1994. Pulsed Infrared Imaging: A New NDT Methodology for Above Ground Storage Tanks, *Materials Evaluation,* Vol. 52(7), pp. 814-815.
9. B. T. Griffith, D. Turler and H. Goudey, 2002. Infrared Thermography, *Encylcopedia of Imaging Science and Technology,* Vol. 1, J. P. Hornak (ed.), John Wiley & Sons, pp. 802-817.
10. L.W. Kessler, P.R. Palermo, and A. Korpel, 1972. Practical High Resolution Acoustic Microscopy, *Acoustical Holography,* Vol. 4, G. Wade (ed.), New York: Plenum Press, pp. 51-71.
11. R.A. Lemons and C.F. Quate, 1974. Acoustic Microscope—Scanning Version, *Applied Physics Letters,* Vol. 24 (4), pp. 163-165.
12. J. Gould, 1987. An Examination of Nugget Development During Resistance Spot Welding Using Both Experimental and Analytical Techniques, *Welding Journal Research Supplement,* Vol. 67(1), pp. 1s-10s.
13. A.R. Levander, 1988. Fourth-Order Finite-Difference P-SV Seismograms, *Geophysics,* Vol. 53 (11), pp. 1425-1436.

14. J.O.A. Robertsson, 1996. A Numerical Free-Surface Condition for Elastic/Viscoelastic Finite-Difference Modeling in the Presence of Topography, *Geophysics,* Vol. 61 (6), pp. 1921-1934.
15. J.O.A. Robertsson, J.O. Blanch and W.W. Symes, 1994. Viscoelastic Finite-Difference Modeling, *Geophysics,* Vol. 56 (9), pp. 1444-1456.